Acta Polytechnica **63**(1):11–18, 2023
https://doi.org/10.14311/AP.2023.63.0011

Published by the Czech Technical University in Prague

ESTIMATION OF STRESSES IN A MASSIVE GRANITE USING LASER ULTRA-SONIC TESTING AND STRESS MEMORY EFFECT

Ondřej Kašpar[a], Alexander Kravcov[b,*], Jiří Štoller[c], Petr Kubeček[b], Radovan Vnuk[b], Zbyněk Zušťák[b]

[a] *Charles University in Prague, Faculty of Science, Engineering Geology and Applied Geophysics, Albertov 6, 128 43 Prague 2, Czech Republic*

[b] *Czech Technical University in Prague, Faculty of Civil Engineering, Department of Construction Technology, Thákurova 7, 160 00 Prague, Czech Republic*

[c] *University of Defence in Brno, Faculty of Military Technologies, Kounicova 65, 662 10 Brno, Czech Republic*

[*] corresponding author: kravtale@fsv.cvut.cz

Abstract. This paper addresses in-situ stress-estimation methods based on the Kaiser effect. The physical and mechanical properties of granite, diorite, and granodiorite samples selected at different depth intervals of the core obtained from a wellbore were examined. The ultimate uniaxial compressive strength, modulus of elasticity, and Poisson's ratio of the rock samples were determined using presses and strain gauges. Also, local longitudinal and shear wave velocities were measured using a high-accuracy laser-ultrasonic system with a view to assessing the structure of the samples. Based on the resulting elastic wave velocity maps, samples with no obvious discontinuities were chosen. These undisturbed samples were subjected to uniaxial compression and their acoustic emission was simultaneously measured. In-situ stresses were estimated from the results of the interpretation of acoustic emission measurements. The experimental in-situ stresses were compared with the results of a numerical simulation. The ratio of the estimated in-situ stresses to the calculated ones is within the range from 0.81 to 1.11. This means that the laser ultrasonic and acoustic emission methods make it possible to effectively estimate in-situ stresses in a rock mass and assess the degree of rock mass damage.

Keywords: Rock cores, acoustic emission, laser ultrasonic method, structure, stress state, rocks, Kaiser effect.

1. Introduction

Rocks are heterogeneous media that contain defects at different scales; this may cause crack initiation even at light loads [1]. That is why mining operations should be preceded by a detailed study of the geological and geotechnical conditions and analysis of the stress state of the rock mass [2, 3]. Note that one of the main methods for studying the stress state is numerical simulation [4–6]. This is due to the fact that there are no direct methods for measuring in-situ stresses in a rock mass. However, the results of a numerical simulation need to be verified, which is usually done with indirect methods. These are borehole methods, such as hydrofracturing, borehole stress relief, analysis of the erosion of the walls of boreholes, as well as methods for estimating in-situ stresses using core samples (strain recovery analyses, core disking, and acoustic emission testing based on the Kaiser effect). Also, there are methods for stress control in rock outcrops (rock stress relief through the use of hydraulic pads and slots) and analyses of large-scale geological structures (analyses of focal mechanisms of earthquakes and shear displacements) [7–9]. Each of these methods works at a certain scale, which depends on the volume of the rock mass examined. For example, the acoustic methods require the volume of the rock sample to be in the order of 10-3 m^3. On the recommendation of the International Society for Rock Mechanics (ISRM) [10], two downhole methods have been widely adopted: hydraulic fracturing (HF) and complete stress relief. However, these methods are quite complicated and very costly; therefore, alternative methods for determining in-situ stresses are required.

One of the optimal methods for studying in-situ stresses in a rock mass is the method of acoustic emission (AE) [11–14] based on the Kaiser effect [15, 16]. Importantly, this method does not require high-accuracy deformation measurements.

The Kaiser effect describes the phenomenon that repeated loading cycles cause the level of AE signals decrease up to their complete absence until the level of the previously applied load is exceeded [17, 18]. A sharp increase is observed when approaching the previously achieved maximum value of load [12]. Therefore, the repeated loading of samples recovered from different depths makes it possible to estimate the respective in-situ stresses from a sharp increase in the acoustic emission [17, 18]. For this purpose, the Felicity ratio is introduced in [17] and [18], which is the ratio of the load at which acoustic emission (AE) pulses reappear to the maximum load of the previous

load cycle. This ratio can be either greater than 1 or less, depending on the structural and textural features of rock samples, the directions of the principal stresses in the rock mass and other parameters [19–21]. In work [22], data on the seismic wave velocities are used to estimate Young's modulus and Poisson's ratio, in [23], the damage characterisations of granites were studied by a combination of AE and ultrasonic transmission methods under a quasi-static uniaxial compression test. Mechanical characteristics and failure prediction of cement mortar with a sandwich structure was investigated in [24]. In studies [25–29], acoustic emission is used for understanding the mechanical properties of materials.

The value of the Felicity ratio changes in response to an increase in the time interval between loading cycles, which may make the effect less distinct. The duration of stress memory also depends on the rock type, the loading regime in successive cycles, and the effect of other factors (heating and moistening). Moreover, some rocks retain information on the experienced mechanical stresses for many months, or even years. That is why it is important to study and identify patterns of AE activity inside one type of rocks.

In this study, we investigate if it is possible to estimate in-situ stresses in a granite mass using acoustic emission observed during uniaxial compression of core samples preliminarily examined in structural terms using laser ultrasonic methods.

2. Materials and methods

2.1. Materials

To assess the possibility of using the method of acoustic emission when studying the stress-strain state of a rock mass, granite samples taken from a core sample while drilling a well in the crystalline massif from depths from 70 m to 400 m were studied.

Sample PB1-11 (depth 95.5 m) is grey, heterogeneous, fine-to-medium-grained, dense, massive granodiorite containing inclusions of light-coloured minerals and thin long healed cracks running through the sample;

Sample PB1-32 (depth 95.5 m) is dark pink with a greyish tinge, medium-to-coarse-grained, dense, massive granite interspersed with dark-coloured minerals and thin cracks no more than 1.5 cm long in places;

Sample PB1-56 (depth 230.2 m) is dark pink, heterogeneous, fine-to-medium-grained, dense, massive granite with a large number of inclusions of dark-coloured minerals (> 20 %) and occasional inclusions of mica; no visible cracks are present;

Sample PB1-80 (depth 302.0 m) is light pink with a greyish tinge, fine-to-medium-grained, dense, massive granite interspersed with inclusions of biotite (no more than 5 %); solitary thin cracks no more than 1 cm long are present;

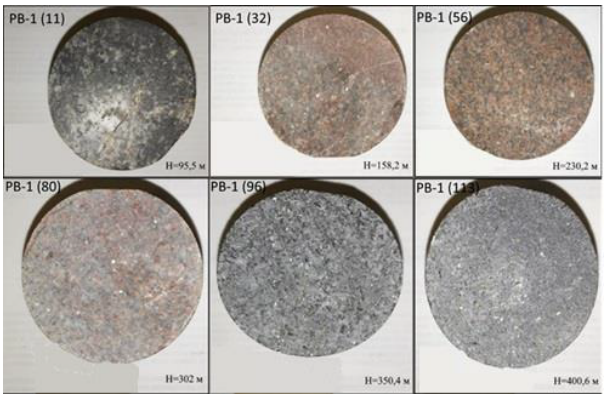

Figure 1. Samples of granite from crystalline massif.

Sample PB1-96 (depth 350.4 m) is dark grey, medium-to-fine-grained, dense, massive diorite interspersed with dark-coloured minerals and inclusions of mica (about 5 %); no visible cracks are present; and

Sample PB1-113 (depth 400.6 m) is dark grey, fine-grained, dense, massive diorite interspersed with dark-coloured minerals and inclusions of mica (about 5-7 %); no visible cracks are present.

Figure 1 shows six granite samples recovered from different depths.

Cylindrical specimens about 10 cm long and about 6 cm in diameter were prepared from these samples. The volume V and density ρ of the specimens were determined.

According to the research, it was found that granodiorites of fine-grained structure, dense and massive, with healed cracks noted (according to sample PB1-11), belong to the migmatite-plagiogranite formation. They are composed of plagioclase, quartz, and biotite in variable amounts – hornblende, epidote, microcline. The structure of the rock shows elements of gneiss and taxite appearance and without metallogenic prospects.

One typical photograph of granite is presented in Figure 2 (No. 2). The samples are presented slightly different in composition, structure (PB1-32 – coarse-medium-grained, PB1-56 and 80 – fine-medium-grained) and patterns of relationship with the rocks of the enclosing frame by species and varieties. Unlike granodiorites, they are two-feldspar rocks with higher silicic acidity and potassium alkalinity.

There are two pictures of diorites (No. 3 – medium-grained and No. 4 – fine-grained) – these samples include plagioclase, hornblende, biotite, as well as apatite, garnet, epidote, chlorite, ore (magnetite, sulphides) in the smallest proportions. Texturally dense, massive, structurally intact.

2.2. Ultrasonic measurements

First, it was necessary to select specimens without long internal cracks which could relieve the stress the specimens experienced in situ; in that case, information

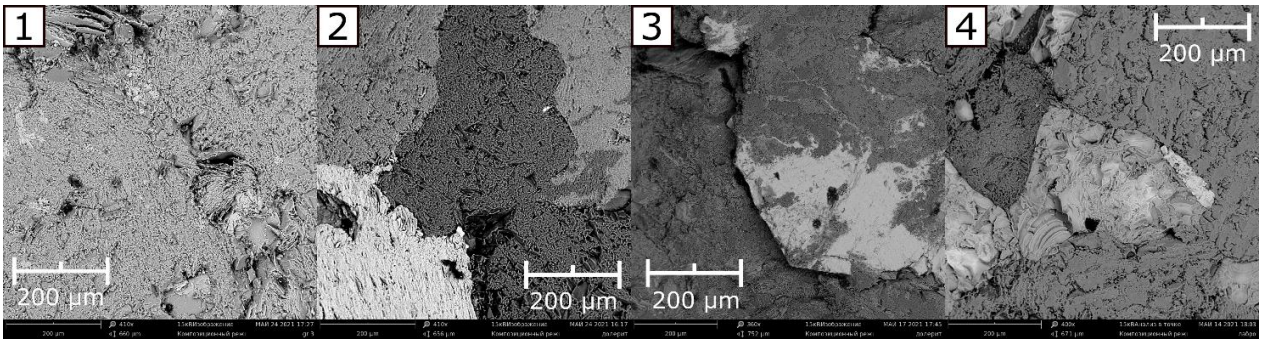

FIGURE 2. Results of microscopic study of characteristic polished sections of each sample of rocks – grano-diorite (No. 1 – PB1-11), granite (No. 2 – PB1-32 / 56/80) and diorites (No. 3 and 4 – PB1-113 and PB1-96) using a Phenom ProX scanning electron microscope.

about these stresses may get lost. To check the "homogeneity" of the specimens, they were scanned using a laser-ultrasonic flaw detector operating in an automatic pulse-echo mode. Figure 3 shows a schematic diagram of scanning. A laser optoacoustic transducer excites a short powerful longitudinal wave pulse. At the transducer-specimen interface, the longitudinal wave is partially converted into shear wave. Both waves are reflected from the diametrically opposite generatrix of the specimen and recorded by a broadband piezoelectric transducer (Figure 3). Their velocities are calculated from the time delay of the waves for a given sample diameter. The measurement error of elastic wave velocities was 0.2 % [21]. Scanning was carried out along the generatrix with a step of 1 cm. Longitudinal wave velocity maps produced using the MatLab software were used for a visual inspection of the specimens to find out if there are large-scale defects such as cracks/pores larger than 5 mm in size. Also, the dynamic Young's modulus E_d and shear modulus G, and Poisson's ratio ν were calculated from the velocities using the formula [21]:

$$E_d = \rho \cdot V_p^2 \cdot \left[3 - \frac{1}{\chi^{-1}}\right], \tag{1}$$

$$G = \rho \cdot V_s^2, \tag{2}$$

$$\nu = \frac{\chi^{-2}}{2 \cdot (\chi^{-1})}, \tag{3}$$

where G is the shear modulus, ρ is the density, and $\chi = (\frac{\nu_p}{\nu_s})^2$ is the square of the ratio of longitudinal wave velocity to shear wave velocity.

2.3. MECHANICAL TESTING

The physical and mechanical properties of the specimens (ultimate uniaxial compressive strength R_c, static modulus of elasticity E, and Poisson's ratio ν) were determined with the use of TP-1-1500 press with

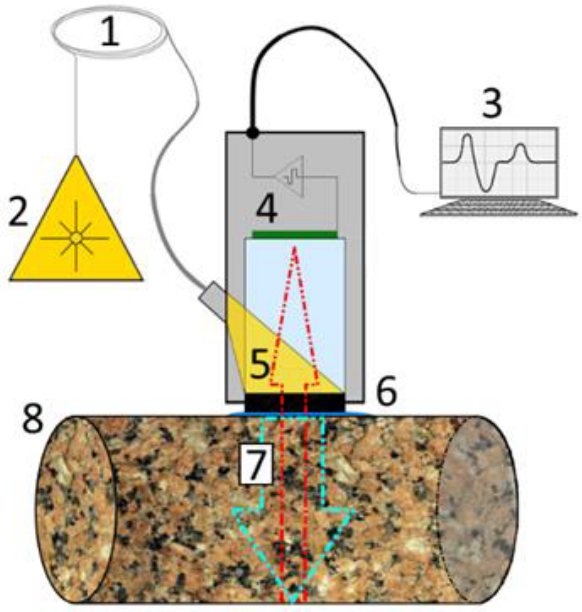

FIGURE 3. Schematic diagram of measurement of elastic wave velocities using laser ultrasonic flaw detector: optical cable (1), laser (2), computer (3), detector (4), laser radiation (5), optoacoustic generator (6), pulses (7), granite specimen (8).

a maximum load of 1500 kN and a tensometric complex consisting of an LTR crate system and ACTEST-OEM software (modules LTR 212M-2 and LTR-EU-2-5). The press and the tensometric complex were synchronised to stress recording. Then, longitudinal and lateral compressive strains were measured as the specimens were subjected to load changing from 5 % to 50 % of the ultimate compressive strength.

2.4. ACOUSTIC EMISSION MEASUREMENTS

The memory effect was studied with a SDS 1008 acoustic emission monitoring system and Maestro 1.2.2 software for data processing. The cumulative AE count Nand acoustic emission activity C_Σ were analysed [1].

№	h_{abb} [m]	h [cm]	d [cm]	m [g]	V [cm^3]	ρ [g cm^{-3}]	V_p [m s^{-1}]	V_S [m s^{-1}]	ν	E [GPa]	R_c [MPa]
1	74,6	9,83	6,26	864,19	308,2	2,78	6018	3774	0,21	102	51
2	95,5	9,99	6,3	881,03	315,2	2,76	5490	2998	0,22	72	94
3	150	10,31	6,3	847,48	325,3	2,61	5253	3096	0,23	72	158
4	158,2	10,19	6,3	833,13	321,5	2,59	5673	3067	0,22	84	150
5	201,2	10,24	6,29	839,46	322,1	2,61	5523	3106	0,27	80	191
6	212,2	9,94	6,29	823,75	313,6	2,63	5696	3443	0,21	85	195
7	230,2	11,74	6,3	908,62	370,4	2,57	6485	3781	0,24	103	195
8	260	10,43	6,26	853,73	326	2,62	6052	3507	0,25	96	146
9	302	10,31	6,3	850,54	326,3	2,61	5627	3124	0,28	83	175
10	350,4	10,16	6,28	925,96	319,6	2,85	5971	3467	0,25	103	116
11	400,6	10,31	6,28	925,8	326,3	2,78	5764	3044	0,31	94	149

Table 1. Physical and mechanical properties of specimens.

3. Results

The physical and mechanical properties of the specimens are shown in Table 1.

According to Table 1, the specimens are hard; the highest values of rock skeletal density are typical of granodiorite and diorite ($\rho = 2.81$–$2.90\,\mathrm{g\,cm^{-3}}$) unit, the density of granite specimens (ρ) varies from 2.57 to $2.63\,\mathrm{g\,cm^{-3}}$; the dynamic modulus of elasticity varies from 72 to 103 GPa. The hardest granite is found in the middle of the analysed depth interval (from 200 to 230 m).

The specimens were subjected to uniaxial compression and their acoustic emission was simultaneously recorded.

The rocks in the massif were in stress state, so the goal of acoustic emission testing was to estimate in-situ stresses and compare them with the results of a numerical simulation. However, since available archive materials do not have the level of detail that is required for a numerical simulation, the vertical stresses in the rock mass were calculated under the assumption that rock stress changes with depth as a result of geostatic load, according to which the expression for vertical stresses is as follows

$$\sigma = \rho\, g\, h, \tag{4}$$

where h_{abb} is the depth. Accordingly, horizontal stresses can be estimated in terms of the parameters presented in Table 1:

$$\sigma = \xi\, \rho\, g\, h, \tag{5}$$

where ξ is the lateral earth pressure coefficient:

$$\xi = \frac{\nu}{(1-\nu)}, \tag{6}$$

where ν is Poisson's ratio.

In this approximation, vertical and horizontal stresses were calculated with respect to the borehole axis.

Figure 4 shows longitudinal velocity maps for Specimens No. 4 and No. 5 (given in Table 1). Specimens C and D (sample depths of 157.1 and 200.3 m, respectively) were discarded due to the considerable variation of the P-wave velocity. Specimen C has a variation coefficient of 3.5 %, and specimen D of 2.1 %. A total of 54 velocity values were determined for each specimen (the grid of scanning was 9 by 6 points). Specimens A and B were homogeneous and structurally undisturbed; so they were investigated using the acoustic emission method.

Stress calculations were performed for granite, diorite, and granodiorite, which are igneous rocks; they are characterised by similar structural-textural features and similar behaviour under load. The resulting values of vertical and horizontal stresses are given in Table 2. The third column of the table contains the names of the specimens subjected to uniaxial compression accompanied with simultaneous recording of acoustic emissions.

Figure 5 shows the calculated distribution of the stress with depth (based on Table 2).

The specimens mentioned in Table 2 were subjected to uniaxial compression and acoustic emission was simultaneously recorded. It was found that the experimental relationship between stress and AE count is similar to that determined from theoretical experiments aimed at recovering in-situ stresses in different types of granite. Figure 6 shows the cumulative number of AE events (AE count N) versus the applied load (Specimen PB1-50). Calculated by the above formula, the averaged vertical stress at the sampling depth of PB1-50 is equal to 5.44 MPa. Using inflection of the experimental AE count versus stress curve (Figure 6), the in-situ stress the specimen experienced is estimated at 5.56 MPa; so the Felicity ratio is $FR = 1.02$. Thus, the error of in-situ stress estimation is 2 %.

The AE testing of Specimen PB1-113 produced similar results. Figure 6 shows the AE activity (Σ) versus the applied load for this sample. Clearly, two differently inclined tangents can be drawn to the AE

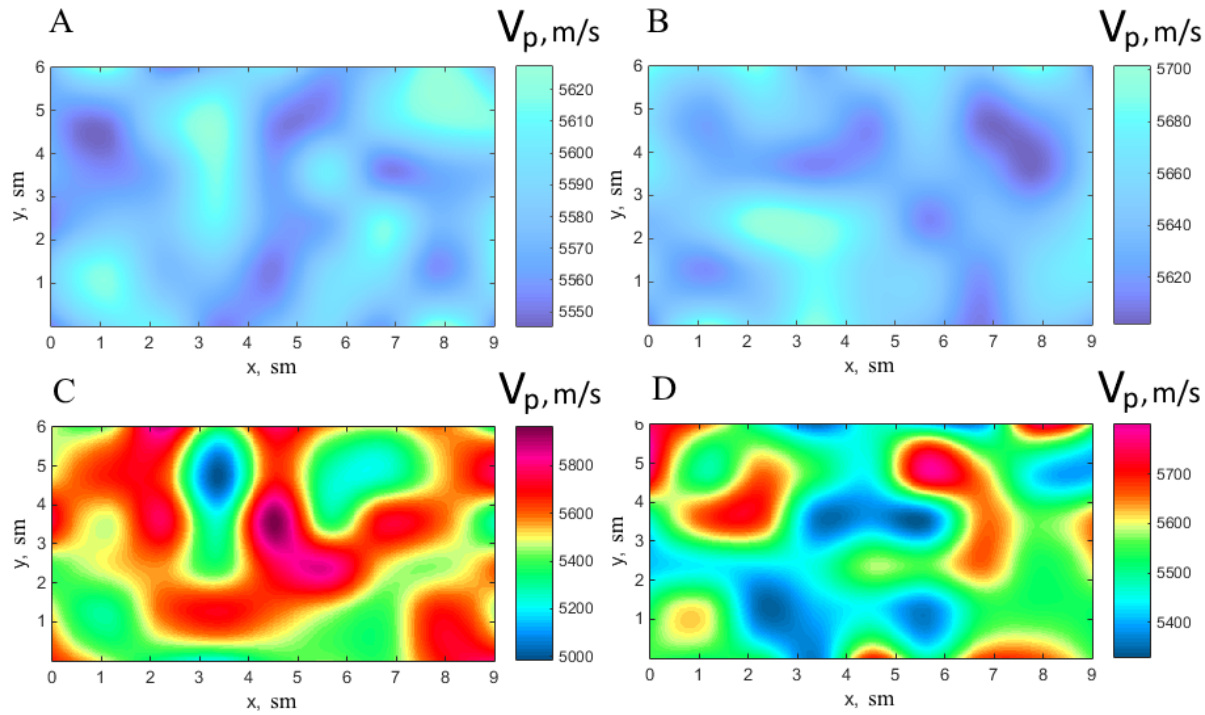

FIGURE 4. Velocity distributions: homogeneous specimens (A and B) and heterogeneous specimens (C and D).

Depth h from [m]	to	**Specimen №**	ρ [$g\,cm^{-3}$]	ν	ξ	[MPa]	[MPa]	**Rock type**
0	20,5		2,01	0,29	0,69	0,40	0,69	quaternary sediments
20,5	44,0		2,63	0,22	0,28	1,01	0,28	granite
44,0	74,8	PB1-4(74.6 m)	2,78	0,21	0,27	1,84	0,49	granite
74,8	95,7	PB1-11(95.5 m)	2,76	0,22	0,28	2,41	0,64	granodiorite
95,7	107,0		2,78	0,21	0,27	2,73	0,72	granodiorite
107,0	119,5		2,63	0,22	0,28	3,05	0,86	granite
119,5	121,8		2,58	0,33	0,49	3,11	1,53	granite
121,8	145,0		2,63	0,22	0,28	3,71	1,05	granite
145,0	150,2	PB1-29(150.0 m)	2,61	0,23	0,49	3,83	1,89	granite
150,2	153,0		2,58	0,33	0,49	3,91	1,93	granite
153,0	158,4	PB1-32(158.2 m)	2,59	0,22	0,28	4,04	1,14	granite
158,4	177,3		2,63	0,22	0,28	4,54	1,28	granite
177,3	193,7		2,64	0,21	0,28	4,96	1,40	granite
193,7	201,4	PB1-46(201.2 m)	2,61	0,29	0,41	5,15	2,10	granite
201,4	208,6		2,61	0,29	0,41	5,34	2,18	granite
208,6	212,4	PB1-50(212.2 m)	2,62	0,28	0,40	5,43	2,22	granite
212,4	228,2		2,61	0,29	0,41	5,84	2,38	granite
228,2	230,4	PB1-56(230.2 m)	2,65	0,20	0,25	5,89	1,47	granite
230,4	260,2	PB1-66(260.0 m)	2,65	0,20	0,25	6,67	1,67	granite
260,2	302,4	PB1-80(302.2 m)	2,65	0,20	0,25	7,76	1,94	granite
302,4	302,7		2,65	0,20	0,25	7,78	1,94	diorite
302,7	305,0		2,61	0,32	0,47	7,83	3,69	diorite
305,0	350,6	PB1-96(350.4 m)	2,65	0,20	0,25	9,01	2,25	diorite
350,6	400,6	PB1-113(400.6 m)	2,65	0,20	0,25	10,32	2,58	diorite

TABLE 2. The most intense UV-Vis spectral lines of SM-I and its investigated derivatives.

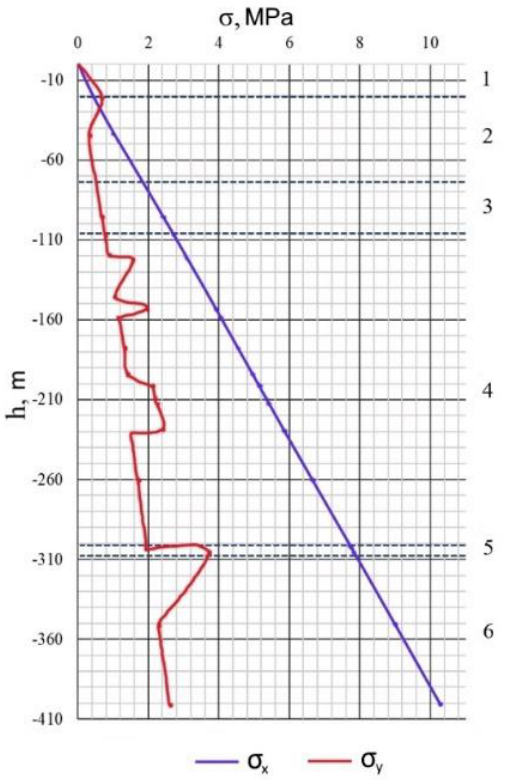

Figure 5. Distribution of averaged vertical and horizontal stresses with depth (deformation properties ignored) along the borehole axis: Quaternary sediments (1), granite (2), granodiorite (3), and granite (4); zone of higher level of fracturing (5); diorite (6) Quaternary sediments (1); granite (2); granodiorite (3); granite (4); zone of higher level of fracturing (5); diorite (6).

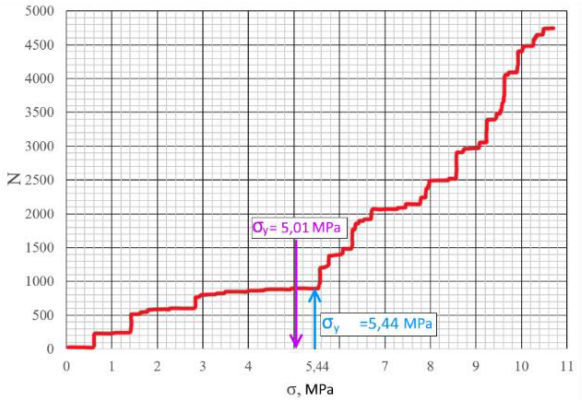

Figure 6. Cumulative AE count versus stress (Specimen PB 1-50): recovered in-situ stress value (purple arrow – approximate value of stresses acting in the array; blue arrow – the value of the restored voltage).

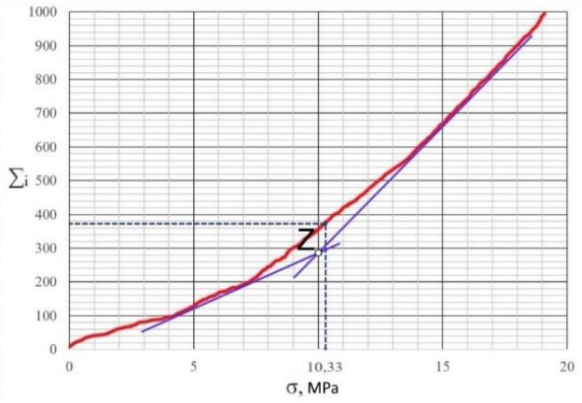

Figure 7. Cumulative AE count versus stress (specimen PB 1-113).

activity versus the applied load curve. The coordinate of the intersection of these tangent lines corresponds to the value of the in-situ vertical stress the specimen experienced before its recovery from the borehole. So, based on the results of AE testing of this sample, the vertical in-situ stress is 10.33 MPa, the stress memory factor being equal to 0.97 (based on numerical simulations, the vertical in-situ stress is 10.00 MPa). Note that this sample demonstrates a classical example of estimating the stress memory effect using the generally accepted technique of drawing tangents to linear sections of the AE count (N) vs. stress plot (point Z is the intersection of the tangents in Figure 7).

4. Discussion

Thus, in the case of specimen PB1-50 (granite), the stress memory effect is manifested by a significant increase in the AE count after the applied load has exceeded the previously experienced stress, which was observed in theoretical experiments as well. Specimen PB1-113 (diorite) did not show such a pattern; therefore, it was required that tangents be drawn. This is most likely due to lithological differences between the specimens.

Table 3 shows the values of calculated vertical stress σ_y and vertical stress $\sigma_y^{estimated}$ recovered from AE measurements, and the Felicity ratio FR_y. Clearly, except for a depth of 95.5-95.7 m, the values of the Felicity ratio are close to 1, belonging to the interval [0.81; 1.12], which indicates that the principal in-situ stress can be recovered.

5. Conclusions

The acoustic emission method based on the Kaiser effect has some advantages over other in-situ stress estimation methods. The method is an efficient and easy-to-use one. No complex high-precision deformation measurements are required. It is quite reasonable to use this AE method for studying the stress state of a rock mass. The method is very informative, describing in detail how the distribution of stress with depth depends on the structure of the rock mass.

Acknowledgements

This study was financially supported by the research team from the National Ministry of the interior of the Czech Republic VB01000057 and the authors also want to express their gratitude to the Czech Technical University in Prague for the grants No. 211453T11 and No. 211473T11.

Depth h from [m]	to	Specimen №	σ_y [MPa]	$\sigma_y^{estimated}$ [MPa]	FR_y
74,6	74,8	4	1,85	2,29	0,81
95,5	95,7	11	2,42	1,36	1,55
150,0	150,2	29	3,84	3,82	1,00
158,2	158,4	32	4,05	-	-
201,2	201,4	46	5,15	6,18	0,83
212,2	212,4	50	5,44	5,54	0,99
230,2	230,4	56	5,90	5,25	1,12
260,0	260,2	66	6,67	6,78	0,98
302,2	302,4	80	7,77	9,62	0,81
350,4	350,6	96	9,02	-	-
400,6	400,8	113	10,32	10,0	0,96

TABLE 3. Estimation of in-situ stresses using the AE method.

REFERENCES

[1] Y. A. Kashnikov, S. G. Ashikhmin, A. E. Kukhtinskii, D. V. Shustov. The relationship of fracture toughness coefficients and geophysical characteristics of rocks of hydrocarbon deposits. *Journal of Mining Institute* **241**:83, 2020. https://doi.org/10.31897/pmi.2020.1.83

[2] M. A. Karasev, M. A. Buslova, M. A. Vilner, T. T. Nguyen. Method for predicting the stress-strain state of the vertical shaft lining at the drift landing section in saliferous rocks. *Journal of Mining Institute* **240**:628, 2019. https://doi.org/10.31897/pmi.2019.6.628

[3] I. A. Shibaev, I. E. Sas, E. B. Cherepetskaya, D. M. Bagryantsev. Substantiation of possible simplifications in the assessment of soil-foundation interaction. *Mining informational and analytical bulletin* (9):152–157, 2018. https://doi.org/10.25018/0236-1493-2018-9-0-152-157

[4] X. F. Li, Q. B. Zhang, H. B. Li, J. Zhao. Grain-based discrete element method (GB-DEM) modelling of multi-scale fracturing in rocks under dynamic loading. *Rock Mechanics and Rock Engineering* **51**:3785–3817, 2018. https://doi.org/10.1007/s00603-018-1566-2

[5] H. Munoz, A. Taheri. Specimen aspect ratio and progressive field strain development of sandstone under uniaxial compression by three-dimensional digital image correlation. *Journal of Rock Mechanics and Geotechnical Engineering* **9**(4):599–610, 2017. https://doi.org/10.1016/j.jrmge.2017.01.005

[6] F. Wu, Y. Deng, J. Wu, et al. Stress–strain relationship in elastic stage of fractured rock mass. *Engineering Geology* **268**:105498, 2020. https://doi.org/10.1016/j.enggeo.2020.105498

[7] B. Amadei, O. Stephansson. *Rock Stress and its Measurement*. Chapman & Hall, London, Great Britain, 1997.

[8] J. Sjöberg, R. Christiansson, J. A. Hudson. ISRM suggested methods for rock stress estimation – Part 2: overcoring methods. *International Journal of Rock Mechanics and Mining Sciences* **40**(7):999–1010, 2003. https://doi.org/10.1016/j.ijrmms.2003.07.012

[9] A. Zang, O. Stephansson. *Stress Field of the Earth's Crust*. Springer, Potsdam, Germany, 2010, p 321.

[10] B. C. Haimson, F. H. Cornet. ISRM suggested methods for rock stress estimation – Part 3: hydraulic fracturing (HF) and/or hydraulic testing of pre-existing fractures (HTPF). *International Journal of Rock Mechanics and Mining Sciences* **40**(7):1011–1020, 2003. https://doi.org/10.1016/j.ijrmms.2003.08.002

[11] A. Lehtonen, J. W. Cosgrove, J. A. Hudson, E. Johansson. An examination of *in situ* rock stress estimation using the Kaiser effect. *Engineering Geology* **124**:24–37, 2012. https://doi.org/10.1016/j.enggeo.2011.09.012

[12] A. Lavrov. Fracture-induced physical phenomena and memory effects in rocks: A review. *Strain* **41**(4):135–149, 2005. https://doi.org/10.1111/j.1475-1305.2005.00233.x

[13] Z.-H. Zhang, J.-H. Deng. A new method for determining the crack classification criterion in acoustic emission parameter analysis. *International Journal of Rock Mechanics and Mining Sciences* **130**:104323, 2020. https://doi.org/10.1016/j.ijrmms.2020.104323

[14] E. Zezulová, K. Hasilová, T. Komárková, et al. NDT methods suitable for evaluation the condition of military fortification construction in the field. *Applied Sciences* **10**(22):8161, 2020. https://doi.org/10.3390/app10228161

[15] V. L. Shkuratnik, Y. L. Filimonov, S. V. Kuchurin. Acoustic emission memory effect in coal samples under uniaxial cyclic loading. *Journal of Applied Mechanics and Technical Physics* **47**:236–240, 2006. https://doi.org/10.1007/s10808-006-0048-6

[16] R. Yu, Y. Tian, X. Wang. Relation between stresses obtained from Kaiser effect under uniaxial compression and hydraulic fracturing. *Rock Mechanics and Rock Engineering* **48**(1):397–401, 2015. https://doi.org/10.1007/s00603-014-0573-1

[17] GOST R 55045-2012 Technical diagnostics. Acoustic emission diagnostics: Terms, definitions, and designations, Moscow, 2014.

[18] ISO 12716:2001 Non-destructive testing – Acoustic emission inspection – Vocabulary ISO/TC 135/SC 9 Acoustic emission testing.

[19] Y. Zhang, Y. Chen, R. Yu, et al. Effect of loading rate on the Felicity effect of three rock types. *Rock Mechanics and Rock Engineering* **50**:1673–1681, 2017. https://doi.org/10.1007/s00603-017-1178-2

[20] Y. Tian, R. Yu, Y. Zhang. Application of Felicity effect in crack stress identification and quantitative damage assessment of limestone. *Rock Mechanics and Rock Engineering* **53**:2907–2913, 2020. https://doi.org/10.1007/s00603-020-02062-x

[21] A. I. Sagaydak, V. V. Bardakov, S. V. Elizarov, V. I. Ivanov. Standards for the technical state testing of reinforced concrete structures by means of acoustic emission method. *Testing Diagnostics* (06):32–39, 2020. https://doi.org/10.14489/td.2020.06.pp.032-039

[22] N. N. Melnikov, S. P. Mesyats, S. P. Ostapenko, et al. Investigation of disturbed rock zones in open-pit mine walls by seismic tomography. In *Structural and Mechanical Engineering for Security and Prevention*, vol. 755 of *Key Engineering Materials*, pp. 147–152. Trans Tech Publications Ltd, 2017. https://doi.org/10.4028/www.scientific.net/KEM.755.147

[23] G. K. Zhang, H. B. Li, M. Y. Wang, X. F. Li. Crack initiation of granite under uniaxial compression tests: A comparison study. *Journal of Rock Mechanics and Geotechnical Engineering* **12**(3):656–666, 2020. https://doi.org/10.1016/j.jrmge.2019.07.014

[24] X. Liu, Q. Gu, Y. Tan, et al. Mechanical characteristics and failure prediction of cement mortar with a sandwich structure. *Minerals* **9**(3):143, 2019. https://doi.org/10.3390/min9030143

[25] I. A. Shibaev, V. A. Vinnikov, G. D. Stepanov. Determining elastic properties of sedimentary strata in terms of limestone samples by laser ultrasonics. *Mining Informational and Analytical Bulletin* (7):125–134, 2020. https://doi.org/10.25018/0236-1493-2020-7-0-125-134

[26] T. Y. Guo, L. N. Y. Wong. Microcracking behavior of three granites under mode I loading: Insights from acoustic emission. *Engineering Geology* **278**:105823, 2020. https://doi.org/10.1016/j.enggeo.2020.105823

[27] J. Kluczyński, L. Śnieżek, A. Kravcov, et al. The examination of restrained joints created in the process of multi-material FFF additive manufacturing technology. *Materials* **13**(4):903, 2020. https://doi.org/10.3390/ma13040903

[28] A. N. Kravcov, A. Konvalinka, V. A. Vinnikov, et al. On the issue of typical grain size assessment by the methods of broadband laser opto-acoustics. In *Structural and Mechanical Engineering for Security and Prevention*, vol. 755 of *Key Engineering Materials*, pp. 212–218. Trans Tech Publications Ltd, 2017. https://doi.org/10.4028/www.scientific.net/KEM.755.212

[29] J. Li, Y. Huang, Z. Chen, et al. Particle-crushing characteristics and acoustic-emission patterns of crushing gangue backfilling material under cyclic loading. *Minerals* **8**(6):244, 2018. https://doi.org/10.3390/min8060244